2021

Discrimination of immune cell activation using Ramanmicro-spectroscopy in anin-vitro & ex-vivo model

Neha Chaudhary

Thi Nguyet Que Nguyen

Daniel Cullen

See next page for additional authors

Authors
Neha Chaudhary, Thi Nguyet Que Nguyen, Daniel Cullen, Aidan Meade, and Claire Wynne

Spectrochimica Acta Part A: Molecular and Biomolecular Spectroscopy xxx (xxxx) xxx

Contents lists available at ScienceDirect

Spectrochimica Acta Part A: Molecular and Biomolecular Spectroscopy

journal homepage: www.elsevier.com/locate/saa

Discrimination of immune cell activation using Raman micro-spectroscopy in an *in-vitro & ex-vivo* model

Neha Chaudhary [a,b], Thi Nguyet Que Nguyen [a,b], Daniel Cullen [b,c], Aidan D. Meade [a,b,1], Claire Wynne [c,1,*]

[a] School of Physics, Technological University Dublin, Kevin Street, Dublin 8, Ireland
[b] Radiation and Environmental Science Centre, Focas Research Institute, Technological University Dublin, Kevin Street, Dublin 8, Ireland
[c] School of Biological and Health Sciences, Technological University Dublin, Kevin Street, Dublin 8, Ireland

HIGHLIGHTS

- Raman spectroscopy is an effective method for the differentiation of immune cells.
- Cell lines and primary cells in both resting and activated states were identified.
- Spectral signatures of molecular expression aligned with reference measurements.
- Potential spectral biomarkers that elucidate the spectral classification were identified.

GRAPHICAL ABSTRACT

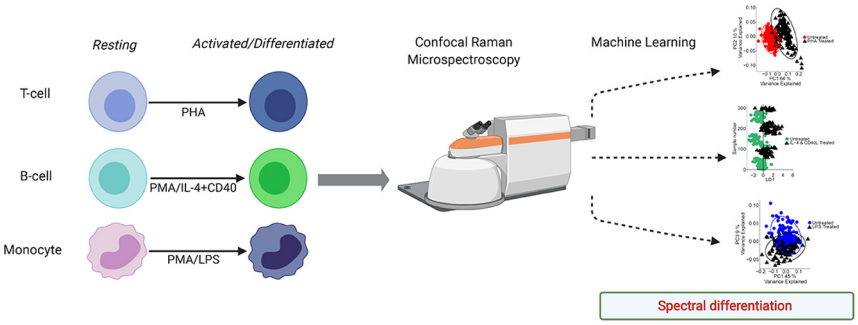

ARTICLE INFO

Article history:
Received 22 July 2020
Received in revised form 14 October 2020
Accepted 16 October 2020
Available online xxxx

Keywords:
Raman spectroscopy
Leucocyte stimulation
Primary cells
Principal component analysis
Linear discriminant analysis

ABSTRACT

Activation and proliferation of immune cells such as lymphocytes and monocytes are appropriate inflammatory responses to invading pathogens and are key to overcoming an infection. In contrast, uncontrolled and prolonged activation of these cellular signalling pathways can be deleterious to the body and result in the development of autoimmune conditions. The understanding of cellular activatory status therefore plays a significant role in disease diagnosis and progression. Conventional automated approaches such as enzyme linked immunosorbent assays (ELISA) and immune-labelling techniques are time-consuming and expensive, relying on a commercially available and specific antibody to identify cell activation. Developing a label-free method for assessing molecular changes would therefore offer a quick and cost-efficient alternative in biomedical research. Here Raman spectroscopy is presented as an effective spectroscopic method for the identification of activated immune cells using both cell lines and primary cells (including purified monocyte and lymphocyte subgroups and mixed peripheral blood mononuclear cell (PBMC) populations) obtained from healthy donors. All cell lines and primary cells were exposed to different stimulants and cellular responses confirmed by flow cytometry or ELISA. Machine learning models of cell discrimination using Raman spectra were developed and compared to reference flow-cytometry, with spectral discrimination levels comparing favourably with the reference method. Spectral signatures of molecular expression after activation were also extracted with results demonstrating alignment with expected profiles. High performance classification models constructed in these *in-vitro* and *ex-vivo* studies enabled identification of the spectroscopic discrimination of immune cell subtypes in their resting and activated state. Further spectral fitting analysis identified a number of potential spectral biomarkers that elucidate the spectral classification.

* Corresponding author at: School of Biological and Health Sciences, Technological University Dublin, Kevin Street, Dublin 8, Ireland.
E-mail address: claire.wynne@tudublin.ie (C. Wynne).
[1] These authors contributed equally to this work.

https://doi.org/10.1016/j.saa.2020.119118
1386-1425/

1. Introduction

Inflammation is a recognised hallmark of many clinical disorders and involves a coordinated response of innate and adaptive immune cells against invading pathogens [1]. The innate immune response provides a rapid and non-specific reaction to the presence of foreign pathogens but lacks memory while the adaptive immune response which is characterised by a slow, challenge-specific response, creates an immunological memory after an initial encounter with a specific pathogen. The innate immune response is mediated by innate immune cells which include mast cells, natural killer (NK) cells, eosinophils, basophils and phagocytic cells (including monocytes, macrophages, neutrophils, and dendritic cells (DCs)). The adaptive immune response is mainly mediated by T and B lymphocytes.

Previously, it had been considered that the innate and adaptive arm of the immune network were independent defence mechanisms, with the innate immune system recognising foreign pathogens non-specifically [2]. It has long been accepted that there is significant bidirectional cooperativity between the innate and adaptive immune response, with many studies describing their crosstalk and the potential to exploit this to develop therapies for various diseases [2–4]. In a functional immune system, the biochemical events which transduce pro-inflammatory signals from infected tissue cause the recruitment of monocytes from the bone marrow. These monocytes differentiate into phagocytic macrophages and along with DCs, enter the lymph nodes. The interaction between antigen presenting cells (APCs) such as DCs, and naïve T cells, enhances the adaptive immune response against the pathogen [5]. Cell activation is an early and crucial step in mounting an antigen-dependent or independent stimulation of adaptive and innate immune cells and triggering signalling cascades as a defence mechanism [6]. The intracellular signalling events triggered eventually result in morphological and molecular changes inside the cell and on its surface [7,8].

In general standard reference methods such as ELISA, flow cytometry and confocal microscopy are used to monitor the activation status of immune cells by measuring cytokines released or the expression of specific molecules of interest [9]. These approaches require cellular fixation, chemical staining and fluorescent labelling with conjugated antibodies which are invasive and may interfere with biological processes, thus potentially preventing the accurate investigation of cellular behaviour in a disease state [10].

Raman spectroscopy is a non-invasive, label-free optical technique capable of decoding the biochemical signature of cells and tissues *in-situ*. It relies on the intrinsic scattering characteristics of the molecular composition of the cell under investigation and provides a chemical fingerprint of the cell without the requirement of extrinsic labels such as conjugated antibodies, stains or radioactive labels. This has allowed it to be employed for the development of methods for the automated discrimination of immune cell lines and their subpopulations [10–13], the differentiation of cell lines [14] and drug-cell interactions [10,15], amongst other applications. While examination of the effect of leucocyte stimulation on Raman spectra has been performed previously, no work has compared and contrasted these signals both in immune cell lines and primary leucocytes (both purified cell subgroups and peripheral blood mononuclear cell (PBMC) populations).

In this study Raman spectroscopy was employed for the analysis of immune cells in both resting and activated states using *in-vitro* and *ex-vivo* models, with a specific aim to develop a spectral model of immune cell activation both within leucocyte subpopulations and mixed PBMCs.

2. Materials and methods

2.1. Ethical approval

Ethical approval was awarded by the TU Dublin Ethics Committee (approval REC 16-92) for the conduct of this study. Two 3.5 mL sodium citrate whole blood samples were obtained from each healthy volunteer who had provided informed consent.

2.2. Cell culture

Cells of the Raji B line were a gift from and Dr. David Brayden (University College Dublin, Ireland) while Jurkat T cells and THP-1 monocytes were obtained from existing laboratory stocks. The standard protocol from American Type Culture Collection (ATCC) was followed for the resuscitation of frozen cell lines and their culture. All cell lines were cultured in suspension in Roswell Park Memorial Institute medium −1640 (RPMI); (Sigma Aldrich, Dublin, Ireland), supplemented with 10% foetal bovine serum (FBS) (Sigma Aldrich, Dublin, Ireland) at 37 °C in a humidified atmosphere with 5% CO_2.

PBMCs were isolated from whole blood by gently mixing 3 mL of Dulbecco's modified phosphate buffered saline (DPBS) with 3 mL of blood. This mixture was then overlaid onto 6 mL of Histopaque and separated by centrifugation at 400*g* for 30 min at 18 °C with brakes off. The PBMC layer was pipetted off and the supernatant discarded. These cells were re-centrifugated and washed in DPBS three times before the pellet was resuspended in RPMI supplemented with 12.5% FBS and cultured at 37 °C, 5% CO_2.

2.3. Cell treatment

All cell lines were seeded at a density of 5×10^5 cells/mL in a final volume of 2 mL in a 6-well plate (Nunc, Fisher Scientific, Ireland) for treatment, with parallel samples prepared for flow cytometry and Raman spectroscopy. Jurkat T cells were treated with phytohaemagluttinin (PHA) (10 μg/mL) (Sigma Aldrich, Dublin, Ireland) for 24 hr [16] and Raji B cells with 20 ng/mL phorbol 12-myristate 13-acetate (PMA, Sigma Aldrich, Dublin, Ireland) and 0.3 μM Ionomycin (Sigma Aldrich, Dublin, Ireland) for 48 hr [17]. THP1 monocytes were treated with 100 nM PMA at 37 °C in 5% CO_2 for 72 hr to induce macrophage differentiation [18]. After the exposure period had elapsed, samples were washed with the appropriate media after centrifugation at 300*g* for 5 min.

PBMCs were treated with either PHA (10 μg/mL for 72 hr) or LPS (0.1 μg/mL for 24 hr). Purified monocyte and lymphocyte subpopulations were obtained from each whole blood sample using the EasySep Direct Human T cell, B cell and monocyte isolation kits (Stemcell Technologies, Grenoble, France) following the manufacturer's recommended protocol. This step was performed within 4 hr of blood collection. All primary cells were seeded at a density of 5×10^5 cells/mL in a 24-well plate (Nunc, Fisher Scientific, Ireland). T lymphocytes were treated with 10 μg/mL PHA for 72 hr [16], B lymphocytes with 0.08 μg/mL IL-4 and 2 μg/mL CD40 ligand (CD-40L) for 48 hr [19] and monocytes with 0.1 μg/mL lipopolysaccharide (LPS; Sigma Aldrich, Dublin, Ireland) for 24 hr [20]. At the end of the treatment time, cells were washed with DPBS after centrifugation at 300*g* for 5 min and their response assessed using flow cytometry, ELISA and Raman spectroscopy.

2.4. Flow cytometry

Flow cytometry was conducted using a BD Biosciences Accuri C6 Flow Cytometer (Becton Dickinson, Oxford, UK). The washed

cell pellet was blocked in PBS solution supplemented with 2% FBS for 30 min at 4 °C. After blocking, cells were resuspended in 10 μL of conjugated monoclonal antibody and 200 μL of blocking solution (PBS supplemented with 2% FBS) for 30 min at 4 °C. Cell purity was measured with fluorescent staining for monoclonal antibodies for each leucocyte subtype (anti-human CD14 as a monocyte marker (PE, Clone: 63D3), anti-human CD3 as a T cell marker (FITC, Clone: OKT3), anti-human CD19 as a B cell marker (PE, Clone: HIB19)) versus a general leucocyte marker (anti-human CD45 (APC, Clone: HI30) (Medical Supply Co. Ltd, Dublin, Ireland)). The mean fluorescence intensity (MFI) of anti-human CD69 (FITC, Clone: FN50) (Beckton Dickinson BioSciences, Dublin, Ireland) was measured to determine the levels of lymphocyte activation. Cells were washed and resuspended in 200 μL of PBS to remove unbound antibody prior to flow cytometry measurements. A minimum of 10,000 cell events per sample were recorded. Unwanted debris and cell aggregates were excluded from the analysis using proper gating based on forward (FSC) and side scatter (SSC) characteristics.

2.5. Enzyme linked immunosorbent assay

ELISA was used to measure the levels of cytokine expression in both *in-vitro* and *ex-vivo* experiments. In all cases, the supernatant of each sample was collected and stored at −80 °C for further analysis. The expression of TNF-α within the culture media was assessed using a human TNF-α ELISA MAX deluxe kit (BioLegend, Dublin, Ireland) following the manufacturer's recommended protocol. The absorbance of each sample was measured using a SpectraMax M3 Spectrometer/Plate Reader at 450 nm and 570 nm.

2.6. Raman spectroscopy

Cultured cell samples were washed and fixed using 2% paraformaldehyde (PFA) in PBS. Fixed cells were drop cast onto calcium fluoride (CaF_2, Crystan Ltd, Dorset, UK) slides and then washed three times with deionised water. The slides were allowed to air dry for 30 min and were stored in a desiccator at room temperature until the time of measurement.

Raman spectra were acquired with a Horiba Jobin-Yvon LabRam HR 800 system using a 532 nm laser excitation and a diffraction grating of 600 lines/mm, which provided a spectral resolution of ~2 cm^{-1}. The excitation laser power (~12 mW) was delivered via a × 100 objective (MPlanN, Olympus, numerical aperture (NA) = 0.9) giving a spot size of diameter ~0.7 μm. The confocal hole diameter was set to 150 μm and the spectra were recorded with a 20 s integration time averaged over three accumulations over the fingerprint region from 400 to 1800 cm^{-1}. Spectra of thirty to fifty cells were recorded for each sample. Each spectrum was recorded from an individual cell with a 4 × 4 μm raster scan of the centre of each cell including both its nucleus and cytoplasm. All samples were measured within two weeks of slide preparation.

2.7. Spectral preprocessing and analysis

Raman spectral processing algorithms were generated in-house and implemented within the R-based statistical software (Version 1.0.153). Daily wavenumber calibration was performed using the 520.8 cm^{-1} of silicon while multiple calibration spectra of 1,4-Bis (2-methylstyryl) benzene (Sigma Aldrich, Dublin, Ireland) and of the NIST standard SRM 2245 were recorded as a reference before each sample acquisition for wavenumber and intensity calibration in pre-processing.

Spectra were then smoothed (Savitsky-Golay filtration employing a 5^{th} order interpolation polynomial with a window of 15 points), baseline corrected (subtraction of a heavily smoothed spectrum of the sample created using a Savitsky-Golay filter from the sample spectrum followed by a rubberband baseline correction) and vector normalised. Finally outliers were removed (using Rao's statistic with Grubb's test). Principal Component Analysis (PCA) Linear Discriminant Analysis (LDA) models of the spectral data were then developed. Briefly, PCA reformulates the highly covariant spectral variables within matrices of Raman spectra into a new set of mutually orthogonal bases (principal components (PCs) or latent variables (LVs)) and scores. LDA then defines a discriminating line or hyperplane using combinations of PC scores which results in maximum class separation. This approach has been used previously to develop spectral classifiers for disease diagnosis and stratification [21,22]. Here PCA-LDA models were optimised for model performance and complexity (LV) using leave one spectrum out cross-validation (LOOCV). Model performance was expressed in terms of sensitivity and specificity. To enable deeper insight into the biochemical origin of spectral discrimination, classic-least squares (CLS) fitting of spectra was employed. A Raman spectrum of cells may be modelled as a linear combination of spectra of molecular species including protein, lipids and nucleic acid, which exist in the cell at different relative concentrations [23]. Here CLS was performed in Matlab (Version: 9.2.0.556344, R2017a) (Mathworks Inc.) using spectra of pure biochemical species listed in Table 1. Each reference biochemical was purchased from Sigma Aldrich (Ireland) and their spectra were recorded without further purification Examples of these spectra are provided in Supp Figs. 1–3.

Table 1
Pure reference molecules used for CLS analysis in this study.

Category	Pure reference molecules
1) *Amino acids*	Alanine, L-Arginine monohydrochloride, L-Asparagine, L-Aspartic acid, L-Cysteine, L-Cysteine hydrochloride anhydrous, L-Cystine, L-Glutamic acid, L-Glutamine, L-Histidine monohydrochloride, L-Leucine, L-Lysine monohydrochloride, L-Methionine, L-Proline, L-Serine, L-Threonine, L-Valine, L-Phenylalanine, Tryptophan, L-Tyrosine, L-Citrulline, Glycine, Isoleucine, D Aspartic acid, Taurine, Spermine
2) *Protein and related compounds*	Actin, Haemoglobin, Interleukin-8, Clusterin, Ubiquitin, Apolipoprotein E4, Histone, Tumour necrosis factor alpha, Apotransferrin, Lectin, Cytochrome *C*
3) *Nucleic acids and nucleobases*	RNA, DNA, Guanine, Cytosine, Thymine, Uracil, Thymidine, Adenine, Deoxyuridine, Methylcytosine
4) *Growth factors*	Keratinocyte growth factor, Epidermal growth factor
5) *Lipids and fatty acids*	Ceramide, Ceramide 2, Ceramide 14, Ceramide 18, Ceramide 22, Ceramide 24, Linoleic acid, Linolenic acid, Oleic acid, L-Phosphatidylcholine, L-Phosphatidylserine, L- Phosphatidylinositol, L-Phosphatidylethanolamine, Palmitic acid, Sphingomyelin, Stearic acid, Triglyceride
6) *Enzymes*	Carbonic anhydrase, Catalase, Alkaline phosphatase, β-Glucuronidase, Lysozyme, L-Lactate dehydrogenase, DNase 1
7) *Carbohydrate*	Glucose, Glycogen, N-acetyl D-glucosamine
8) *Vitamins*	Biotin, Sodium L-ascorbate, Vitamin C, Vitamin E, Ascorbic acid
9) *Other molecules*	β-Carotene, Uric acid, Creatinine, Xanthine, Lipoic acid, L-Glutathione oxidised, L-Glutathione reduced, Creatinine Anhydrous, Hyaluronic acid, N-acetyl L-cysteine

2.8. Statistical analysis

An unpaired, two-tailed, Students *t*-test was used to ascertain whether statistical significance existed in differences between control and treated samples in respect of MFI and CLS fitting coefficients. This was performed within the R environment (Version 1.0.153) and in Matlab (Version: 9.2.0.556344, R2017a) (Mathworks Inc.).

3. Results

3.1. Discrimination of spectral signatures of immune cell lines in resting and activated states

Combined results from flow cytometry, ELISA (where relevant) and Raman spectroscopy are depicted in Figs. 1–3 respectively for the T lymphocyte (Jurkat), B lymphocyte (Raji-B) and monocyte (THP-1) cell lines. PHA is widely used as an agonist for adaptive immune cells (mainly T lymphocytes) [24]. PHA mainly induces lymphocyte proliferation and evokes cellular compositional changes through the protein tyrosine kinase (PTK) signalling transduction pathway [24,25]. PMA is a specific activator of protein kinase C and hence nuclear factor-kappa-B (NFκB), which has a key role in the inflammatory response while ionomycin is a calcium ionophore which can create similar effects to those seen with TCR-induced phospholipase C activation. Activation of the T and B lymphocyte cell line post treatment was confirmed via a histogram shift – black line (Figs. 1A, 2A respectively) and a significant increase in CD69 expression ((Figs. 1B, 2B respectively), while activation of the THP1 monocyte line was confirmed by a statistically significant increase in TNF-α release post PMA treatment (Fig. 3A).

The Raman mean spectra, PCA scores and the results of CLS fitting of spectra are shown in each figure. The assignment for the individual Raman band of interest is listed (Table 2). In the case of the T lymphocyte cell line the mean Raman spectra of untreated and PHA treated Jurkat T cells exhibited many similar features; however some subtle variations in modes associated with protein were observed (Fig. 1C). A PCA-LDA model was optimised to a complexity of 3 LVs and performed with 91% sensitivity and 70% specificity, respectively, owing to the high intra-sample variability seen in PCA scores within Fig. 1D. CLS analysis identified differentiated spectral contributions from actin, apotransferrin, arachadonic acid, DNA, histone, and proteinase-K (Fig. 1E).

Similarly, in Fig. 2, mean Raman spectra demonstrated that slight alterations in the PMA and Ionomycin treated Raji B lymphocytes occurred in the regions associated with nucleic acid and protein content of the samples (780, 876, 1094, 1315, 1338, 1002, 1576 cm^{-1}) [26] (Fig. 2C). PCA-LDA classification of stimulated from resting Raji B lymphocytes was optimised using the first 6 LVs, performing with sensitivity and specificity of 95.2% and 81.6%, respectively (see PCA scores in Fig. 2D). The CLS fitting of spectra pre and post treatment identified several differentiated molecular species including actin, apotransferrin, arachidonic acid, carbonic anhydrase, DNA, histone, linoleic acid, linolenic acid,

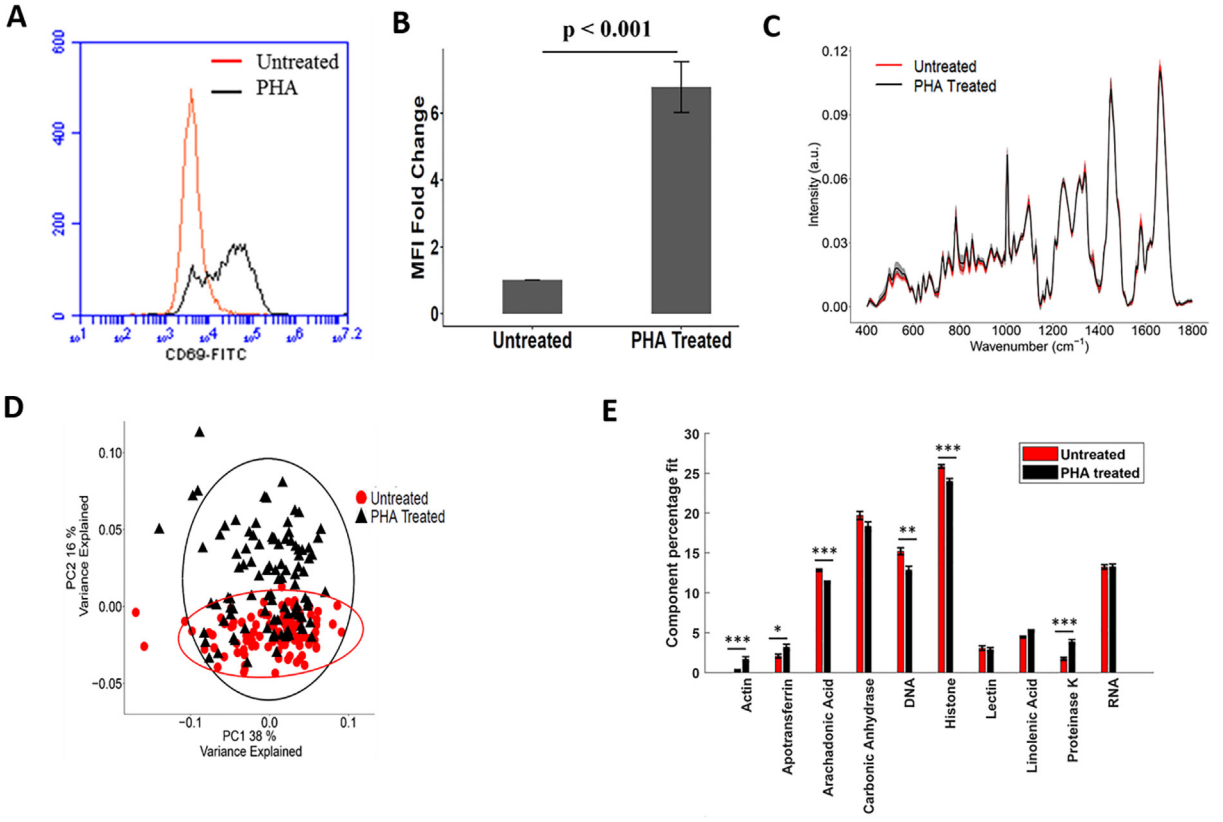

Fig. 1. PHA treatment of Jurkat T cells caused an increase in CD69 expression. (A) The overlay histogram plot shows the expression of CD69 in untreated (red line) and PHA treated cells (black line), (B) Mean Fluorescence Intensity (MFI) produced by CD69 expression on untreated and PHA treated Jurkat cells. Data is normalised to untreated cells and is expressed ± SD (n = 3), (C) Mean and standard deviation of Raman spectra of untreated and PHA treated Jurkat T cells, (D) PCA score plot of Raman spectra of Jurkat T cells in the absence or presence of PHA (10 μg/mL). Percentage label on each axis in (D) indicates the variance associated with the principal component (PC) outlined for the discrimination of untreated and PHA activated Jurkat T cells. Covariance ellipses (95% confidence limit) in (D) are shown for each class. (E) The normalised component fit of pure reference molecules from CLS fitting of Raman spectra of untreated and PHA treated Jurkat T cells. Data is normalised to untreated Jurkat cells and is expressed ± SE (n = 3). Significance is shown in (E) by (*) and indicates a significance of *p < 0.05, **p < 0.001 and ***p < 0.0001.

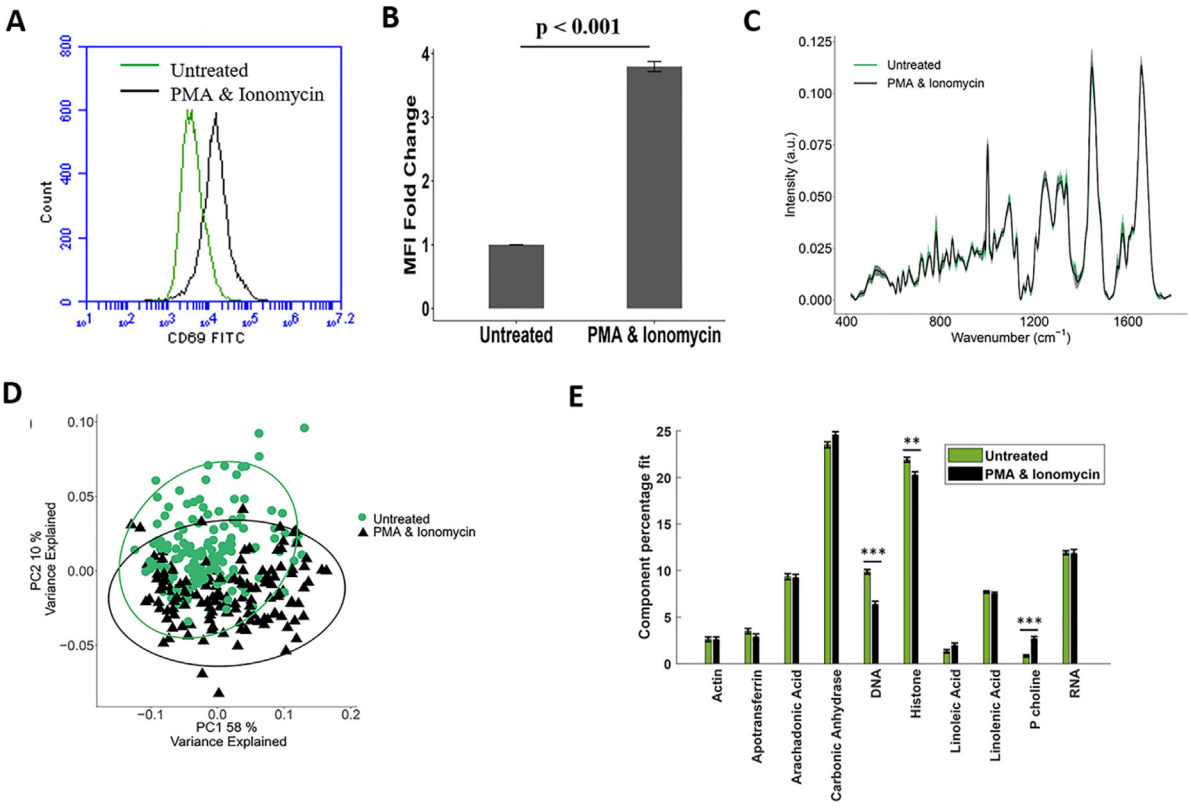

Fig. 2. PMA and ionomycin treatment of Raji B cells caused an increase in CD69 expression. (A) The overlay histogram plot shows the expression of CD69 by untreated (green line) and treated cells (black line). (B) Mean Fluorescence Intensity (MFI) produced by CD69 expression on untreated and PMA and ionomycin treated Raji B cells. Data is normalised to untreated cells and is expressed ± SD (n = 3), (C) Mean and standard deviation of Raman spectra of untreated and PMA and ionomycin treated Raji B cells, (D) PCA score plot of Raman spectra of control and PMA and Ionomycin treated Raji B cells. Percentage label on each axis in (D) indicates the variance associated with the principle component (PC) outlined for the discrimination of untreated and PMA and Ionomycin treated Raji B cells. Covariance ellipses (95% confidence limit) in (D) are shown for each class. (E) The normalised component fit of pure reference molecules from CLS fitting of Raman spectra of untreated and PMA & Ionomycin treated Raji B cells. Data is normalised to untreated cells and is expressed ± SE (n = 3). Significance is shown by (*) and indicates a significance of **p < 0.001 and ***p < 0.0001.

phosphatidyl-choline (denoted 'P-choline' in the figure) and RNA (Fig. 2E). Spectral differences in the intensities of the signatures of DNA, histone and Phosphatidyl-choline was observed.

The mean Raman spectra (Fig. 3B) of untreated and PMA treated THP-1 cells exhibited slight alterations in regions associated with protein (1002, 1208, 1250 cm^{-1}), nucleic acid (780, 827, 1094, 1340, 1578 cm^{-1}) and lipid bands (1300, 1444, 1656 cm^{-1}), although it is hard to see all of these alterations macroscopically. Further in a PCA-LDA model spectra, PMA treated and resting THP1 monocytes were also strongly differentiated as seen in the mean raman spectra (Fig. 3B) and PC scores with a model optimised at 2 LVs and a performance of 91% sensitivity and specificity (Fig. 3C). CLS analysis (Fig. 3D) identified a host of significant differentiated spectra signatures including those of actin, apotransferrin, arachidonic acid, DNA, histone, L-alpha phosphatidylcholine, oleic acid, phosphatidyl-ethanolamine (denoted 'P-ethanolamine' in the figure), RNA, and TNF-α, in partial agreement with the ELISA result here.

3.2. Differentiation of spectral signatures in purified primary immune cell subtypes in resting and activated states

In the *ex-vivo* model high cell purities were achieved following negative selection with a mean purity level of 95.4% (range: 94.4–96.2%) for T lymphocytes, 95.6% (range: 92–98.3%) for B lymphocytes and 95.2% (range: 94–97.5%) for monocytes. CD-40L is a ligand which binds to the cellular membrane resulting in B cell specific stimulation, while IL-4 is a cytokine which stimulates B cell proliferation. LPS is recognised by TLR4 which is present on monocytes and macrophages and recruits the transcription factor NFκB into the nucleus which leads to the production of proinflammatory cytokines such as TNF-α, IL-6 and IL-8 [9].

Activation of T and B lymphocytes, as measured via CD69 expression, demonstrated a histogram shift (Figs. 4A, 5A) with a 15-fold and 5-fold increase in the observed MFI by cell type, respectively, though only the former measurement was found to be statistically significant at $p < 0.05$ (Fig. 4B, 5B). Treatment of THP1 monocytic cells with LPS was found to induce a 5-fold increase in TNF-α release (Fig. 6A).

The mean Raman spectra of untreated and PHA-activated T lymphocytes exhibit strongly differentiating bands in the regions associated with nucleic acid and protein (Fig. 4C). Spectral discrimination of stimulated primary T lymphocytes was found to be strong (see PCA scores in Fig. 4D) where a PCA-LDA model optimised to 2 LVs was found to perform with 90.9% and 98.5%, respectively (Fig. 4D). CLS fitting identified a number of strongly differentiated spectral features including those of apotransferrin, arachadonic acid, carbonic anhydrase, DNA, and phosphatidylcholine (denoted 'P-choline' in the figure), with the levels of phosphatidyl-choline strongly altered (Fig. 4E).

Stimulated primary B lymphocytes did not demonstrate similarly strong spectral discrimination from the untreated cells (Fig. 5C), where a PCA-LDA model was optimised to a complexity of 6LVs and performed with a sensitivity and specificity of 89.9% and 81%, respectively (Fig. 5D). This agrees with the non-significant finding in the MFI fold change flow cytometry results

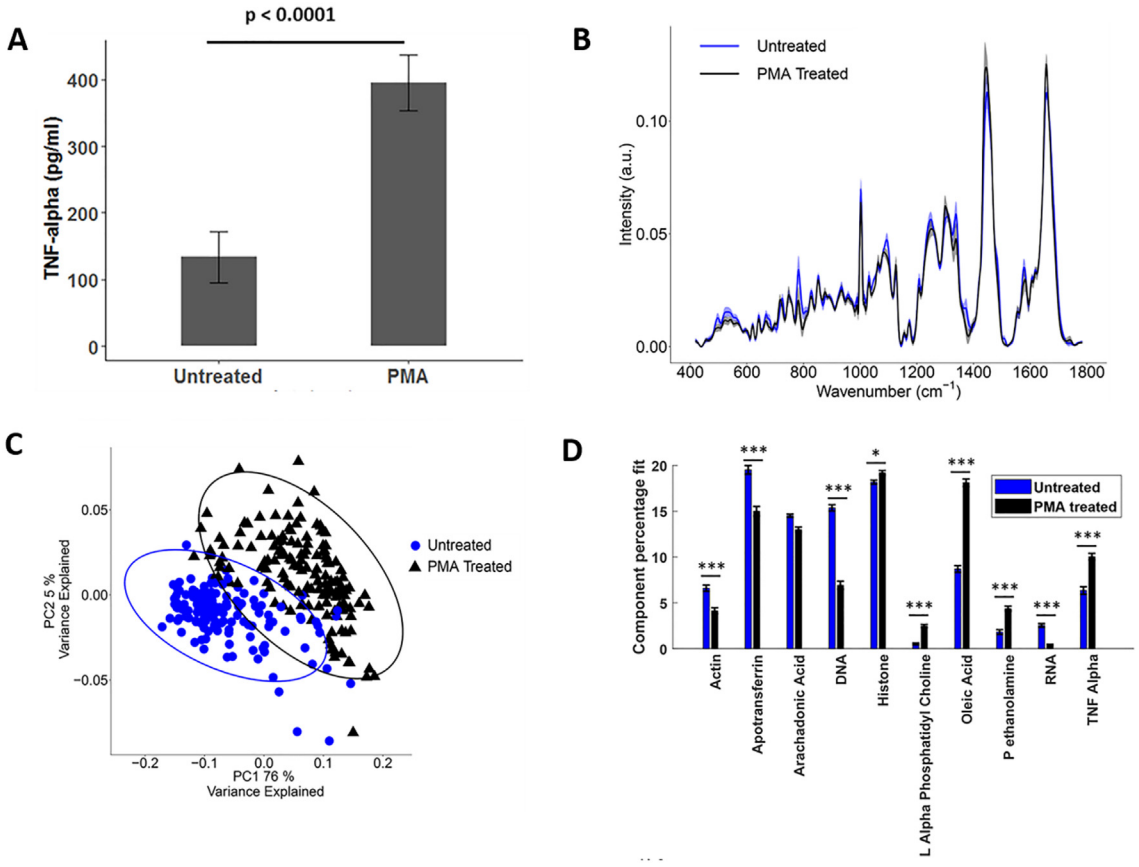

Fig. 3. (A) PMA (100 nM) treatment of THP-1 cells caused an increase in TNF-α production. Data is expressed ± SD, (n = 3), (B) Mean and standard deviation of Raman spectra of untreated and PMA treated THP-1 cells, (C) PCA score plot of Raman spectra of control and PMA treated THP-1 cells. Percentage label on each axis in (C) indicates the variance associated with the principle component (PC) outlined for the discrimination of untreated and PMA treated THP-1 cells. Covariance ellipses (95% confidence limit) in (C) are shown for each class. (D) Normalised component fit of pure reference molecules from CLS fitting of Raman spectra of untreated and PMA treated THP-1 cells. Data is normalised to untreated THP-1 cells and is expressed ± SE (n = 3). Significance is shown by (*) and indicates a significance of *p < 0.05 and ***p < 0.0001.

Table 2
Raman band assignments for some typical vibrations associated with biological specimens.

Frequency (cm^{-1})	Assignment	Frequency (cm^{-1})	Assignment
596	Phosphatidylinositol	1126	C—N stretch (protein)
618	C—C twisting (protein)	1156	C—C, C—N stretch (protein)
646	C—C twisting mode of tyrosine	1194	Nucleic acids and phosphates
678	Guanine ring breathing	1252	Guanine, cytosine
725	Adenine	1280	Amide III
746	Thymine	1300	Fatty acids
780	Uracil ring breathing	1320	CH deformation (proteins) Guanine
790	O—P—O stretching DNA	1373	Thymine, Adenine, Guanine
852	Proline, hydroxyproline, tyrosine	1449	CH_2 bending mode of proteins & lipids
935	C—C stretching mode of proline & valine	1464	Lipids
968	Lipids	1510	Adenine ring breathing
973	C—C backbone (protein assignment)	1552	Tryptophan
980	C—C, =CH stretching (proteins, lipids)	1576	Guanine
1003	Phenylalanine	1650–1680	Amide I
1058	Lipids	1724	Ester group
1096	PO_2^- in nucleic acids	1757	C=O (lipid)

suggesting cells may have only been partially activated. The distribution of LDA scores (Fig. 5D) clearly demonstrated the intergroup variance which exists between unstimulated and CD40L and IL-4 stimulated B lymphocytes according to linear discriminant LD1. The CLS fitting analysis likewise (Fig. 5E) identified only TNF-α and DNA with strongly altered spectral intensities after stimulation.

Finally, the mean Raman spectra of untreated and LPS stimulated monocytes (Fig. 6B), purified from whole blood drawn from healthy volunteers, exhibited slight alterations in regions associ-

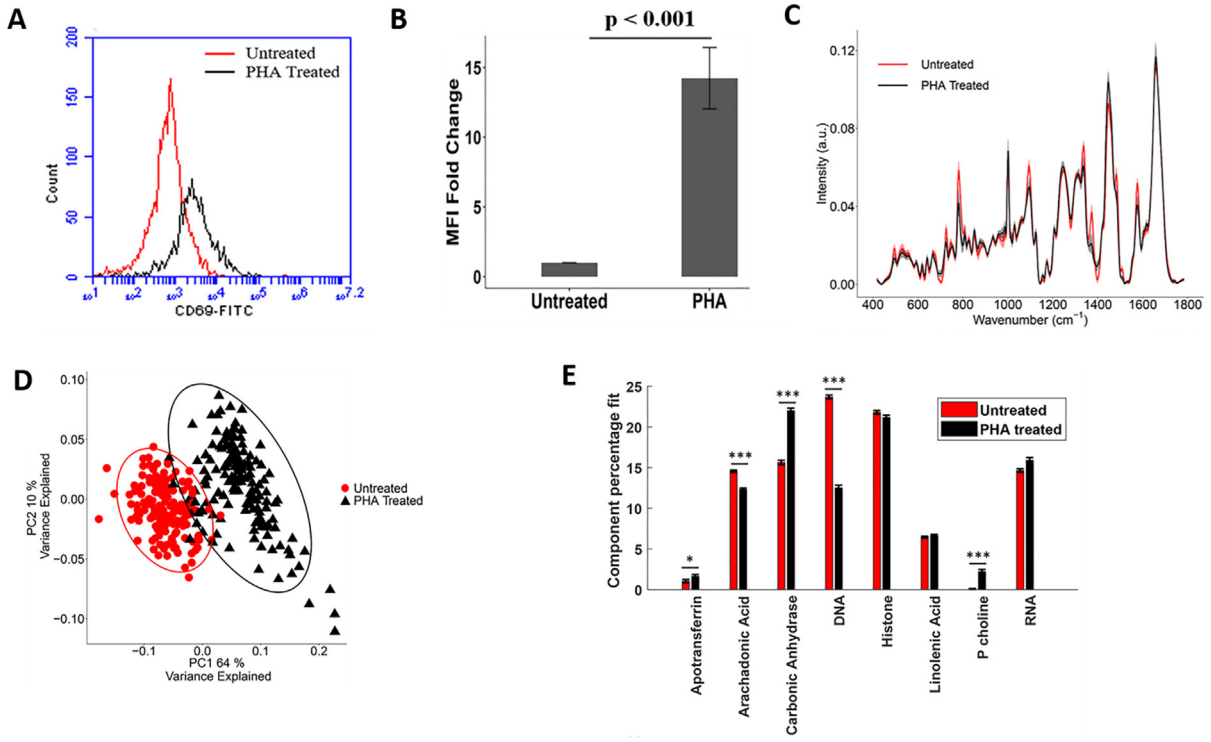

Fig. 4. PHA treatment of T lymphocytes causes an increase in CD69 expression. (A) The overlay histogram plot shows the expression of CD69 on untreated (red line) and PHA treated T lymphocytes (black line). (B) MFI produced by CD69 expression on untreated and PHA treated T lymphocytes. Data is normalised to untreated cells and is expressed ± SD (n = 3). (C) Mean and standard deviation of Raman spectra of untreated and PHA treated T lymphocytes. (D) PCA score plot of Raman spectra of untreated and PHA treated primary T lymphocytes. Percentage label on each axis in (D) indicates the variance associated with the PC outlined for the discrimination of untreated and PHA treated T lymphocytes. Covariance ellipses (95% confidence) in (D) are shown for each class. (E) Normalised component fit of pure reference molecules from CLS fitting of Raman spectra of untreated and PHA treated T lymphocytes. In (E) data is normalised to untreated T lymphocytes and is expressed ± SE (n = 3). Significance is shown by (*) and indicates a significance of $^{*}p < 0.05$, and $^{***}p < 0.0001$.

ated with nucleic acid and protein bands. The differentiation between the spectra of primary monocytes after LPS treatment was reasonably strong with a PCA-LDA model optimised to the first six PCs and delivering a sensitivity of 95.2% and specificity of 80.5% (see PCA scores in Fig. 6C). CLS fitting analysis (Fig. 6D) identified significant changes in arachidonic acid, DNA, histone, linolenic acid and phosphatidyl-ethanolamine (denoted 'P-ethanolamine' in the figure) for the discrimination between the spectra of each class (Fig. 6D).

3.3. Differentiation of spectral signatures of PBMCs in resting and activated states

Within the whole PBMC population, CD69 expression exhibited a histogram shift and a 6-fold increase was observed in the MFI of CD69 following PHA treatment when normalised to untreated cells (Fig. 7A and B), confirming an activation signal which was found to be statistically significant. Similarly ELISA measurements of TNF-α increased 6-fold post LPS treatment, confirming TLR4 engagement and increasing cytokine production (Fig. 8A), which was also found to be statistically significant.

Although not always macroscopically evident, the mean Raman spectra of untreated and PHA treated PBMCs showed variation in modes associated with nucleic acid and protein (Fig. 7C). Spectral discrimination (see PCA scores in Fig. 7D) was strong in the PHA stimulated cells, with PC scores well separated, while a PCA-LDA model was optimised to the first two LVs, delivering sensitivities and specificities of 97.1% and 97.7%, respectively. The CLS fitting analysis identified the spectral signatures of arachidonic acid, carbonic anhydrase, DNA, histone, proteinase-K, RNA and TNF-α as being differentiated to a statistically significantly degree between untreated and stimulated samples (Fig. 7E).

The mean Raman spectra of untreated and LPS treated PBMCs is showin in Fig. 8B. Similarly a PCA-LDA model developed on the spectra of the LPS stimulated PBMC sample was optimised to 3 LVs delivering a sensitivity of 100% and specificity of 90.2% (see PCA scores in Fig. 8C). CLS fitting analysis identified apotransferrin, arachidonic acid, DNA and histone as statistically significantly altered relative to the control (Fig. 8D).

4. Discussion

In general the classification models based on spectral signatures of activated versus resting leucocytes exhibit discrimination performances which align with the level of activation measured by reference methods. Additionally several features regarding the spectral profiles of activated and resting leucocyte subtypes have emerged.

In the first observation it appears that the differentiation between spectral profiles of resting and stimulated cells depends both on the cell type and the simulant itself. Both the Jurkat T cells and primary T cells displayed decreased DNA and histone levels. Upon T cell receptor (TCR) ligand engagement [27,28] a generalised increase in protein phosphorylation is seen, along with a reorganisation of the cytoskeleton and decondensation of nucleic acid within the nucleus of the activated cell [7,25,29–32] which may account for these findings. An increased spectral fit for apotransferrin was also found in both Jurkat T cells and primary T cells upon activation. Previously it has been reported that when stimulated, T cells can synthesise and secrete transferrin [33–35]. An increase in the levels of proteinase-K was observed in Jurkat T cells in which

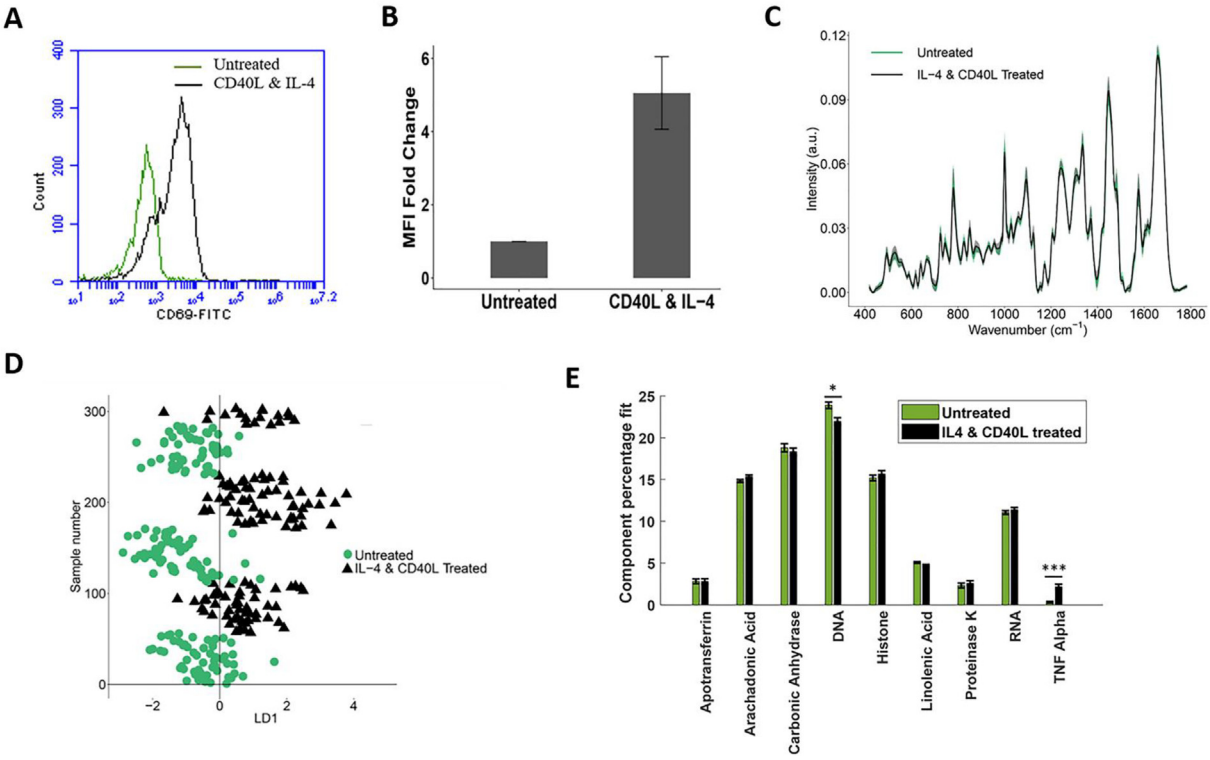

Fig. 5. CD40L and IL-4 treatment of B lymphocytes caused an increase in CD69 expression. (A) The overlay histogram plot shows the expression of CD69 in untreated (green line) and treated cells (black line). (B) MFI produced by CD69 expression of untreated and treated B lymphocytes. Data is normalised to untreated cells and is expressed ± SD (n = 3). (C) Mean and standard deviation of Raman spectra of untreated and CD40L & IL-4 treated B lymphocytes. (D) Scatter plot of PCA-LDA scores of untreated control and CD40L & IL-4 treated B lymphocytes. In (D), each symbol represents a Raman spectra recorded from an individual cell of each group, with each group being denoted by a symbol as shown in the legend. The black line in (D) indicates the hyperplane separating the two groups. (E) Normalised component fit of pure reference molecules from CLS fitting of Raman spectra of untreated and IL-4 & CD40L treated B lymphocytes. Data is normalised to untreated cells and is expressed ± SE (n = 3). Significance is shown in (E) by (*) and indicates a significance of *p < 0.05 and ***p < 0.0001.

the proteolytic activity of proteinase-K is known to increase post PHA treatment due to an increase in intracellular calcium ion (Ca^{2+}) levels promoting downstream cell proliferation [36,37]. This feature was not observed in primary T cells. Conversely the increased levels of phosphatidyl-choline observed in primary T cells, implying increased lipid synthesis as a result of increased cell proliferation [38], is not seen in the Jurkat T cell line, nor is the increased signature of carbonic anhydrase, whose maintenance of intercellular pH level is required for cellular proliferation [39].

In the model of B cell activation two separate stimulants for B cells were employed. Both the Raji-B cell line and primary B cells displayed decreased spectral profiles for DNA levels (Figs. 2E and 5E) post stimulation, again implying association with the decondensation of nucleic acid within the nucleus in response to inflammatory signalling within the cell [7,40]. It is known that the combination of PMA and Ionomycin stimulates protein kinase C (PKC) and raises the level of Ca^{2+} [17], leading to activation of the MAP Kinase superfamily and nuclear translocation of transcription factors such as NFκB resulting in an increase in the protein synthesis rate which ultimately promotes cell proliferation [17,41]. While this could explain the increased contribution of phosphatidyl-choline to Raji B spectra owing to the cross-linking of B cell surface immunoglobulin receptors inducing the breakdown of phosphatidyl-choline in the cell membrane [41,42], this feature was not observed in the primary B cells treated with a different stimulant. Here a significant increase in spectral contribution from TNF-α was observed, which has been observed previously [43–45], but which was not observed in Raji-B cells exposed to ionomycin and PMA. This could be related to the fact that stimulation with IL-4 & CD40L mimicks the T cell dependent activation of B lymphocytes and activates the NFκB signalling pathway which results in the production of TNF-α [46], which is a more specific form of activation in comparison to ionomycin and PMA. This exemplifies the conclusion that the differential mode of action of stimulants are observable spectroscopically.

In the THP-1 monocyte cell line and primary monocytes a number of spectral features increase markedly in both cell types post PMA or LPS treatment (Figs. 3D and 6D), particularly those of lipid origin including phosphatidyl-ethanolamine. The increased levels of phosphatidyl-choline observed in primary monocytes was not observed in THP-1 cells. This may be linked to increasing lipid metabolism, [47,48], or an increase in the presence of leucocyte lipid bodies in cell signalling and inflammation [9,49]. Previous studies have demonstrated that monocyte to macrophage differentiation leads to profound changes in lipid metabolism which prepares the cells for phagocytic and inflammatory function [9,49,50]. The differentiation of monocytic THP-1 cell lines using PMA has also been shown to result in increased adherence and lower rates of proliferation [18]. This may contribute to the CLS fitting results showing a decrease in the spectral features of DNA in the differentiated THP-1 and primary cells, which is corroborated by a time-course LPS activation study of monocytes conducted by Topfer *et al.* [9]. Conversely a decrease in apotransferrin level, which may be attributed to a decrease in transferrin receptor (TfR) expression and transferrin binding, was observed in the stimulated THP-1 cells [51,52] but not the primary cell line. Additionally the spectral features of TNF-α increased post PMA treatment in the THP-1 cell line which align with earlier PMA-induced differentiation studies [53,54], and with the ELISA analysis of the cell supernatant.

In the second observation the spectral profiles of stimulated PBMCs are discriminated when compared to purified stimulated

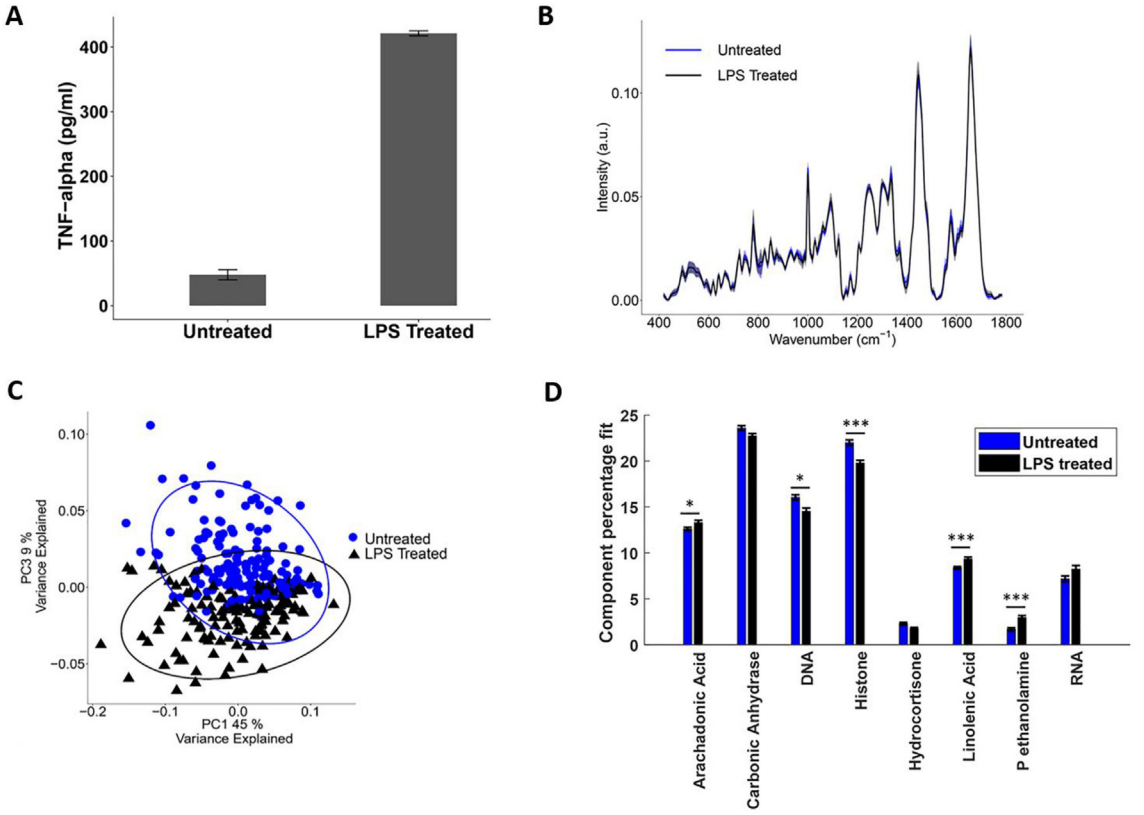

Fig. 6. (A) LPS (0.1 μg/ml) treatment of monocytes caused an increase in human TNF-α release. Data is expressed ± SD (n = 2). (B) Mean and standard deviation of Raman spectra of untreated and LPS treated monocytes. (C) PCA score plot of Raman spectra of untreated and LPS treated monocytes. Percentage label on each axis in (C) indicates the variance associated with the PC outlined for the discrimination of untreated and LPS treated monocytes. Covariance ellipses (95% confidence) in (C) are shown for each class. (D) Normalised component fit of pure reference molecules from CLS fitting of Raman spectra of untreated and LPS treated monocytes. Data is normalised to untreated monocytes and is expressed ± SE (n = 3). Significance is shown in (D) by (*) and indicates a significance of *p < 0.05 and ***p < 0.0001.

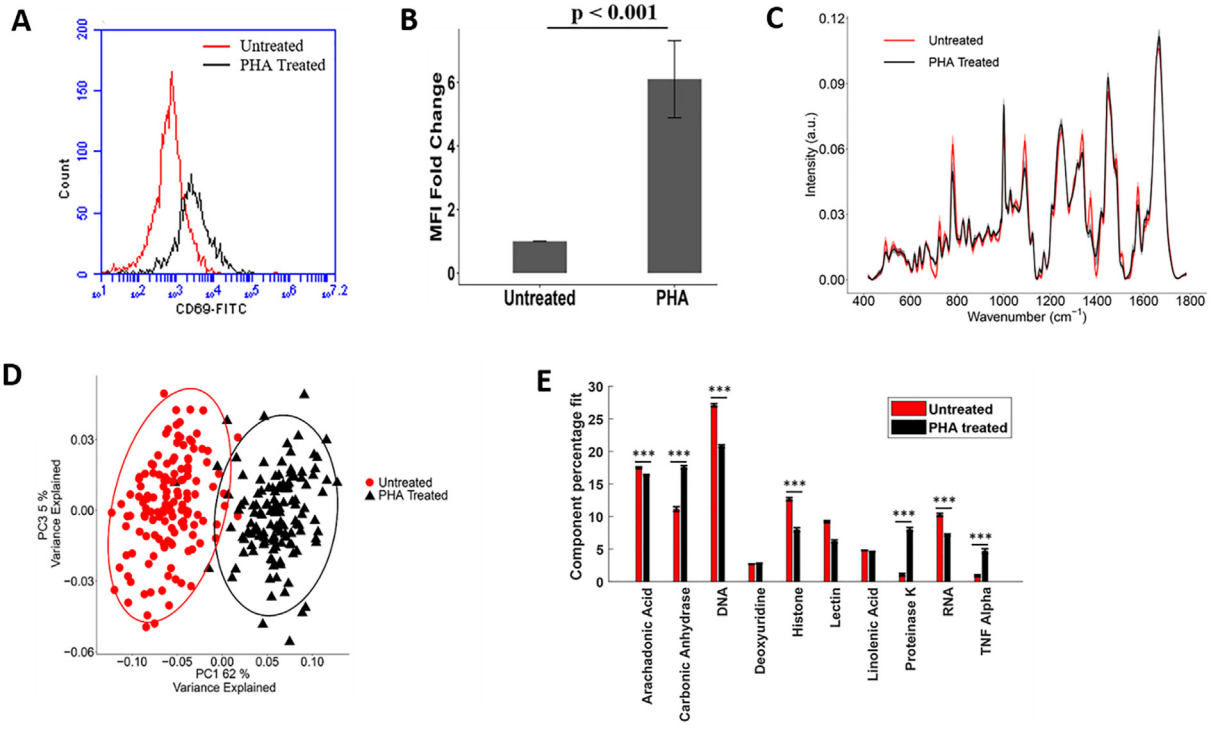

Fig. 7. PHA treatment of PBMCs causes an increase in CD69 expression. (A) The overlay histogram plot shows the expression of CD69 on untreated (red line) and PHA treated PBMCs (black line). (B) MFI produced by CD69 expression on untreated and PHA treated PBMCs. Data is normalised to untreated cells and is expressed ± SD (n = 3). (C) Mean and standard deviation of Raman spectra of untreated and PHA treated PBMCs, (D) PCA score plot. Percentage label on each axis in (D) indicates the variance associated with the PC outlined for the discrimination of untreated and PHA treated PBMCs. Covariance ellipses (95% confidence) in (D) are shown for each class. (E) The percentage component fit of pure reference molecules from CLS fitting of Raman spectra of untreated and PHA treated PBMCs. Data is normalised to untreated PBMCs and is expressed ± SE (n = 3). Significance is shown in (E) by *** and indicates a significance of p < 0.0001.

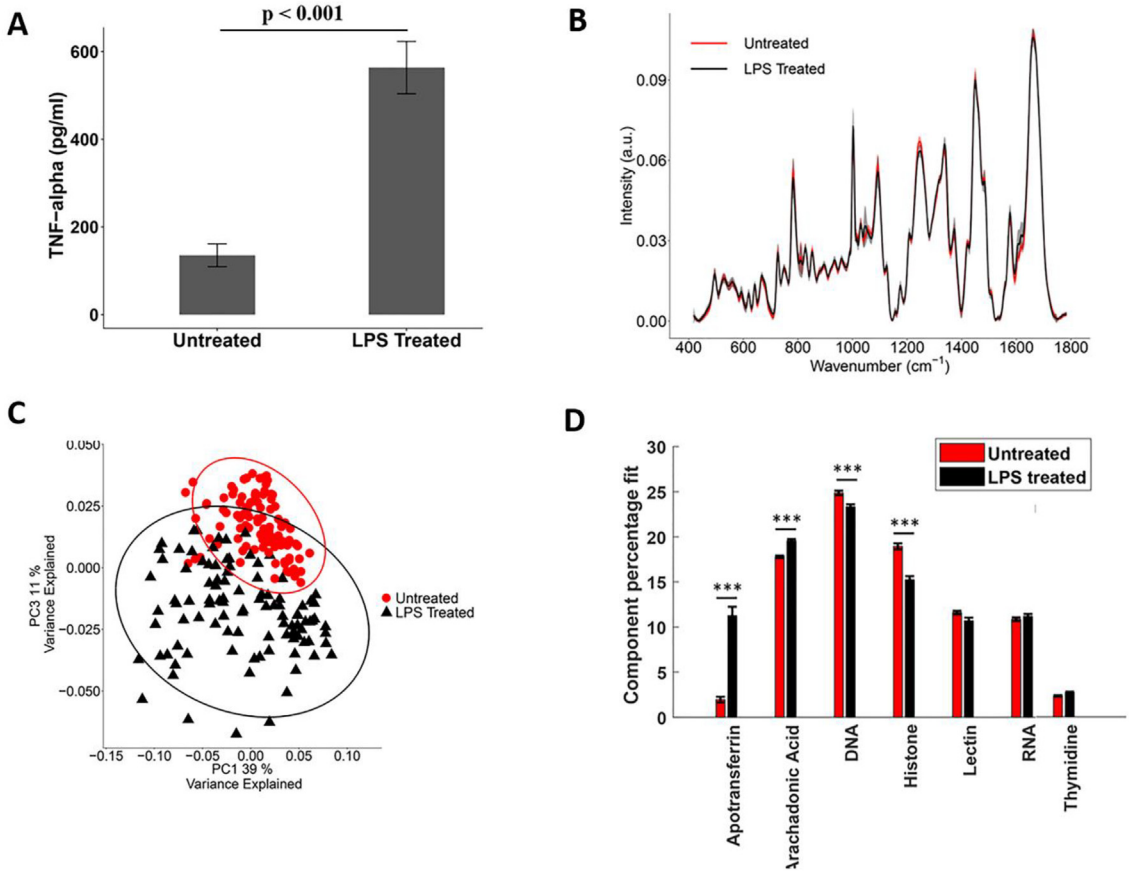

Fig. 8. (A) LPS treatment of PBMCs caused an increase in TNF-α release. TNF-α concentration of untreated and LPS (0.1 μg/ml) treated PBMCs. Data is expressed ± SD. (n = 3). (B) Mean and standard deviation of Raman spectra of untreated and LPS treated PBMCs, (C) PCA score plot. Percentage label on each axis in (C) indicates the variance associated with then PC outlined for the discrimination of untreated and LPS treated PBMCs. Covariance ellipses (95% confidence) in (C) are shown for each class. (D) The percentage component fit of pure reference molecules from CLS fitting of Raman spectra of untreated and LPS treated PBMCs. Data is normalised to untreated PBMCs and is expressed ± SE (n = 3). Significance is shown in (D) by *** and indicates a significance of $p < 0.0001$.

leucocyte subtypes. This implies that the complex interplay of signalling between leucocytes serves to alter their overall spectral signal when they are mixed together as compared to when immune cells subtypes are purified. Spectral fitting of PHA-stimulated PBMCs suggested elevated contributions from proteinase-K, carbonic anhydrase and TNF-α and decreased contributions from DNA, RNA, lectin and histone. While there are elements of these observations which align with those seen in the PHA stimulated Jurkat T cell line, the increased contribution from TNF-α, which has been observed previously in PHA stimulated PBMCs [55,56], suggests the involvement of macrophages which may imply T cell interaction with monocytes post-stimulation. T cell activation is confirmed via the ~6-fold change in CD69 expression within the sample. Stimulation of PBMCs with LPS resulted in a ~4-fold increase in the levels of secreted TNF-α, confirming monocyte activation/differentiation to macrophages. Spectrally this resulted in a decreased spectral contribution from DNA and histone (Fig. 8D), which aligns with data from studies of Jurkat T cell and Raji B cell lines, and an elevated level of apotransferrin and arachidonic acid does not align with results from THP-1 cell line stimulation. This increase in apotransferrin is also seen in Fig. 1E and previous studies [33,34] and suggests it originates in paracrine stimulation of T cells.

5. Conclusion

Results reported here demonstrated the potential of Raman spectroscopy to detect biochemical changes occurring during the *in-vitro* activation of immune cell lines and *ex-vivo* activation of human immune cells by external stimulants. The CLS fitting analysis suggested a panel of pure reference molecules that may be involved in the activation of immune cells. Further calibration of this approach is warranted. Thus, this study has laid a foundation to understand the biomolecular changes occurring during an activatory/inflammatory model using treatment of cells isolated from healthy individuals.

Data availability statement

The data that support the findings of this study are available from the corresponding author upon reasonable request.

CRediT authorship contribution statement

Neha Chaudhary: Methodology, Investigation, Formal analysis, Writing - original draft. **Thi Nguyet Que Nguyen:** Software. **Aidan D. Meade:** Conceptualization, Supervision, Writing - review & editing, Funding acquisition. **Claire Wynne:** Conceptualization, Supervision, Writing - review & editing.

Declaration of Competing Interest

The authors declare that they have no known competing financial interests or personal relationships that could have appeared to influence the work reported in this paper.

Acknowledgements

This work was conducted with the financial support of a TU Dublin Fiosraigh Research Scholarship and funding from the Health Research Board under Grant Agreement No. HRB-POR-2015-1314 at the ADAPT SFI Research Centre at TU Dublin. The ADAPT SFI Centre for Digital Media Technology is funded by Science Foundation Ireland through the SFI Research Centres Programme and is co-funded under the European Regional Development Fund (ERDF) through Grant # 13/RC/2106.

Appendix A. Supplementary material

Supplementary data to this article can be found online at https://doi.org/10.1016/j.saa.2020.119118.

References

[1] D. Ricklin, J.D. Lambris, Complement in immune and inflammatory disorders: pathophysiological mechanisms, J. Immunol. 190 (2013) 3831–3838, https://doi.org/10.4049/jimmunol.1203487.
[2] P.G. Tipping, Toll-like receptors: The interface between innate and adaptive immunity, J. Am. Soc. Nephrol. 17 (2006) 1769–1771, https://doi.org/10.1681/asn.2006050489.
[3] A. Shanker, F.M. Marincola, Cooperativity of adaptive and innate immunity: implications for cancer therapy, Cancer Immunol. Immunother. 60 (2011) 1061–1074, https://doi.org/10.1007/s00262-011-1053-z.Cooperativity.
[4] T.R. Martin, C.W. Frevert, Innate immunity in the lungs, Proc. Am. Thorac. Soc. 2 (2005) 403–411, https://doi.org/10.1513/pats.200508-090JS.
[5] J.A. Owen, J. Punt, S. Stranford, Kuby Immunology: International Edition, 7th ed., Macmillan Learning, 2013.
[6] K. Godoy-Ramirez, K. Franck, S. Mahdavifar, L. Andersson, H. Gaines, Optimum culture conditions for specific and nonspecific activation of whole blood and PBMC for intracellular cytokine assessment by flow cytometry, J. Immunol. Methods 292 (2004) 1–5, https://doi.org/10.1016/j.jim.2004.04.028.
[7] Z.J. Smith, J.-C.E. Wang, S.A. Quataert, A.J. Berger, Integrated Raman and angular scattering microscopy reveals chemical and morphological differences between activated and nonactivated CD8+ T lymphocytes, J. Bomed. Opt. 15 (2010), https://doi.org/10.1117/1.3443794.
[8] S.-M. Kang, R.W. Compans, Host responses from innate to adaptive immunity after vaccination: molecular and cellular events, Mol. Cells 27 (2009) 5–14.
[9] N. Töpfer, M.M. Müller, M. Dahms, A. Ramoji, J. Popp, H. Slevogt, U. Neugebauer, Raman spectroscopy reveals LPS-induced changes of biomolecular composition in monocytic THP-1 cells in a label-free manner, Integr. Biol. 11 (2019) 87–98, https://doi.org/10.1093/intbio/zyz009.
[10] S. Managò, P. Mirabelli, M. Napolitano, G. Zito, A.C. De Luca, Raman detection and identification of normal and leukemic hematopoietic cells, J. Biophoton. 11 (2017) 1–12, https://doi.org/10.1002/jbio.201700265.
[11] M. Chen, N. McReynolds, E.C. Campbell, M. Mazilu, J. Barbosa, K. Dholakia, S.J. Powis, The use of wavelength modulated raman spectroscopy in label-free identification of T lymphocyte subsets, natural killer cells and dendritic cells, PLoS One 10 (2015) 1–14, https://doi.org/10.1371/journal.pone.0125158.
[12] A.J. Hobro, Y. Kumagai, S. Akirac, N.I. Smith, Raman spectroscopy as a tool for label-free lymphocyte cell line discrimination, Analyst. 141 (2016) 3756–3764, https://doi.org/10.1039/C6AN00181E.
[13] J.W. Chan, D.S. Taylor, T. Zwerdling, S.M. Lane, K. Ihara, T. Huser, Micro-Raman spectroscopy detects individual neoplastic and normal hematopoietic cells, Biophys. J. 90 (2006) 648–656, https://doi.org/10.1529/biophysj.105.066761.
[14] S. Takanezawa, S.I. Morita, Y. Ozaki, Y. Sako, Raman spectral dynamics of single cells in the early stages of growth factor stimulation, Biophys. J. 108 (2015) 2148–2157, https://doi.org/10.1016/j.bpj.2015.03.037.
[15] W.J. Tipping, M. Lee, A. Serrels, V.G. Brunton, A.N. Hulme, Imaging drug uptake by bioorthogonal stimulated Raman scattering microscopy, Chem. Sci. 8 (2017) 5606–5615, https://doi.org/10.1039/c7sc01837a.
[16] C. Ishikawa, H. Kawakami, J.-N. Uchihara, M. Senba, N. Mori, CD69 overexpression by human T-cell leukemia virus type 1 Tax transactivation, Biochim. Biophys. Acta 1833 (2013) 1542–1552, https://doi.org/10.1016/j.bbamcr.2013.03.006.
[17] S. Miyamoto, S.R. Kimball, B. Safer, Signal transduction pathways that contribute to increased protein synthesis during T-cell activation, Biochim. Biophys. Acta – Gene Struct. Expr. 1494 (2000) 28–42, https://doi.org/10.1016/S0167-4781(00)00208-6.
[18] E. Richter, K. Ventz, M. Harms, J. Mostertz, F. Hochgräfe, Induction of macrophage function in human THP-1 cells is associated with rewiring of MAPK signaling and activation of MAP3K7 (TAK1) protein kinase, Front. Cell Dev. Biol. 4 (2016) 1–15, https://doi.org/10.3389/fcell.2016.00021.
[19] E.A. Lefevre, R. Krzysiek, E.P. Loret, P. Galanaud, Y. Richard, Cutting edge: HIV-1 Tat protein differentially modulates the B cell response of naive, memory, and germinal center B cells, J. Immunol. 163 (1999) 1119–1122. http://www.ncbi.nlm.nih.gov/pubmed/10415004.
[20] M. Monguió-Tortajada, M. Franquesa, M.R. Sarrias, F.E. Borràs, Low doses of LPS exacerbate the inflammatory response and trigger death on TLR3-primed human monocytes, Cell Death Dis. 9 (2018), https://doi.org/10.1038/s41419-018-0520-2.
[21] A. Ramoji, U. Neugebauer, T. Bocklitz, M. Foerster, M. Kiehntopf, M. Bauer, J. Popp, Toward a spectroscopic hemogram: Raman spectroscopic differentiation of the two most abundant leukocytes from peripheral blood, Anal. Chem. 84 (2012) 5335–5342, https://doi.org/10.1021/ac3007363.
[22] K.L. Brown, O.Y. Palyvoda, J.S. Thakur, S.L. Nehlsen-Cannarella, O.R. Fagoaga, S. A. Gruber, G.W. Auner, Raman spectroscopic differentiation of activated versus non-activated T lymphocytes: An in vitro study of an acute allograft rejection model, J. Immunol. Methods. 340 (2009) 48–54, https://doi.org/10.1016/j.jim.2008.10.001.
[23] I.W. Schie, L. Alber, A.L. Gryshuk, J.W. Chan, Investigating drug induced changes in single, living lymphocytes based on Raman micro-spectroscopy, Analyst. 139 (2014) 2726–2733, https://doi.org/10.1039/c4an00250d.
[24] C.R. Kleiveland, Peripheral blood mononuclear cells, in: K. Verhoeckx, P. Cotter, I. López-Expósito, C. Kleiveland, T. Lea, A. Mackie, T. Requena, D. Swiatecka, H. Wichers (Eds.), Impact Food Bioact. Heal. Vitr. Ex Vivo Model, Springer International Publishing, New York, 2015, pp. 161–167, https://books.google.ie/books?id=2RfyCAAAQBAJ.
[25] Y. He, D. Zhang, T. Tao, Q. Shen, X. Lu, S. Liu, L. Zhong, Raman spectroscopy and AFM imaging directly reveals the activation-dependent characteristic of T cells, Laser Phys. 24 (2014), https://doi.org/10.1088/1054-660X/24/8/085701.
[26] A. Talari, Z. Movasaghi, S. Rehman, I. Rehman, Raman Spectroscopy of Biological Tissues, Appl. Spectrosc. Rev. (2007) 493–541, https://doi.org/10.1080/05704920701551530.
[27] R.L. Wange, L.E. Samelson, Complex complexes: Signaling at the TCR, Immunity. 5 (1996) 197–205, https://doi.org/10.1016/S1074-7613(00)80315-5.
[28] D. Gil, W.W.A. Schamel, F. Sa, B. Alarco, Recruitment of Nck by CD3 epsilon reveals a ligand-induced conformational change essential for T cell receptor signaling and synapse formation, Cell 109 (2002) 901–912, https://doi.org/10.1016/s0092-8674(02)00799-7.
[29] K.I. Jankowska, E.K. Williamson, N.H. Roy, D. Blumenthal, V. Chandra, T. Baumgart, J.K. Burkhardt, Integrins modulate T cell receptor signaling by constraining actin flow at the immunological synapse, Front. Immunol. 9 (2018) 1–19, https://doi.org/10.3389/fimmu.2018.00025.
[30] K. Lam Hui, S.I. Kwak, A. Upadhyaya, Adhesion-dependent modulation of actin dynamics in Jurkat T cells, Cytoskeleton 71 (2014) 119–135, https://doi.org/10.1002/cm.21156.
[31] J.S. Rawlings, M. Gatzka, P.G. Thomas, J.N. Ihle, Chromatin condensation via the condensin II complex is required for peripheral T-cell quiescence, EMBO J. 30 (2011) 263–276, https://doi.org/10.1038/emboj.2010.314.
[32] A. Ramoji, O. Ryabchykov, K. Galler, A. Tannert, R. Markwart, R.P. Requardt, I. Rubio, M. Bauer, T. Bocklitz, J. Popp, U. Neugebauer, Raman spectroscopy follows time-dependent changes in T lymphocytes isolated from spleen of endotoxemic mice, ImmunoHorizons 3 (2019) 45–60, https://doi.org/10.4049/immunohorizons.1800059.
[33] J.B. Lum, A.J. Infante, D.M. Makker, F. Yang, B.H. Bowman, Transferrin synthesis by inducer T lymphocytes, J. Clin. Invest. 77 (1986) 841–849, https://doi.org/10.1172/JCI112381.
[34] H.D. Soltys, J.I. Brody, Synthesis of transferrin by human peripheral blood lymphocytes, J. Lab. Clin. Med. 75 (1970) 250–257, https://doi.org/10.5555/uri:pii:0022214370900119.
[35] The role of iron in cell proliferation and differentiation, (n.d.). https://sickle.bwh.harvard.edu/iron_differentiation.html (accessed March 20, 2020).
[36] X. Wang, H. Luo, H. Chen, J. Wu, W. Duguid, Role of proteasomes in T cell activation and proliferation, J. Immunol. 160 (1998) 788–801.
[37] L.L. Nohara, S.R. Stanwood, K.D. Omilusik, W.A. Jefferies, Tweeters, woofers and horns: The complex orchestration of calcium currents in T lymphocytes, Front. Immunol. 6 (2015) 1–9, https://doi.org/10.3389/fimmu.2015.00234.
[38] J.W. Brewer, Phospholipids: "Greasing the wheels" of humoral immunity, Biochim. Biophys. Acta 2013 (1831) 642–651, https://doi.org/10.1016/j.bbalip.2012.09.018.
[39] M. Leppilampi, P. Koistinen, E.R. Savolainen, J. Hannuksela, A.K. Parkkila, O. Niemelä, S. Pastoreková, J. Pastorek, A. Waheed, W.S. Sly, S. Parkkila, H. Rajaniemi, The expression of carbonic anhydrase II in hematological malignancies, Clin. Cancer Res. 8 (2002) 2240–2245.
[40] K. Nimura, S.S.P. Rao, J. Xu, S. Jung, A. Pekowska, M. Dose, E. Stevens, E. Mathe, S. Huang, M.A. Ricci, L. Baranello, Y. Zheng, T. Ardori, W. Resch, D. Stavreva, S. Nelson, A. Casellas, E. Finn, C. Gregory, B. Glenn, S. Hilaire, S.M. Johnson, W. Dubois, M.P. Cosma, E. Batchelor, Myc regulates chromatin decompaction and nuclear architecture during B cell activation, Mol. Cell 67 (2017) 566–578, https://doi.org/10.1016/j.molcel.2017.07.013.
[41] H. Fan, T.L. Rothstein, Lymphokine dependence of STAT3 activation produced by surface immunoglobulin cross-linking and by phorbol ester plus calcium ionophore treatment in B cells, Eur. J. Immunol. 31 (2001) 665–671, https://doi.org/10.1002/1521-4141(200102)31:2<665::AID-IMMU665>3.0.CO;2-1.
[42] Y.B. Gándola, S.E. Pérez, P.E. Irene, A.I. Sotelo, J.G. Miquet, G.R. Corradi, A.M. Carlucci, L. Gonzalez, Mitogenic effects of phosphatidylcholine nanoparticles on MCF-7 breast cancer cells, Biomed Res. Int. 2014 (2014) 1–13, https://doi.org/10.1155/2014/687037.
[43] P. Rieckmann, J.M. Tuscano, J.H. Kehrl, Tumor necrosis factor-α (TNF-α) and interleukin-6 (IL-6) in B-lymphocyte function, Methods A Companion Methods Enzymol. 11 (1997) 128–132, https://doi.org/10.1006/meth.1996.0396.

[44] J.S. Rush, J. Hasbold, P.D. Hodgkin, Cross-linking surface Ig delays CD40 ligand- and IL-4-induced B Cell Ig class switching and reveals evidence for independent regulation of B cell proliferation and differentiation, J. Immunol. 168 (2002) 2676–2682, https://doi.org/10.4049/jimmunol.168.6.2676.

[45] M.E. Duddy, A. Alter, A. Bar-Or, Distinct profiles of human B cell effector cytokines: a role in immune regulation?, J. Immunol. 172 (2004) 3422–3427, https://doi.org/10.4049/jimmunol.172.6.3422.

[46] R. Elgueta, M.J. Benson, V.C. De Vries, A. Wasiuk, Y. Guo, R.J. Noelle, Molecular mechanism and function of CD40/CD40L engagement in the immune system, Immunol. Rev. 229 (2009) 152–172, https://doi.org/10.1111/j.1600-065X.2009.00782.x.

[47] O. Quehenberger, A. Armando, D. Dumlao, D.L. Stephens, E.A. Dennis, Lipidomics analysis of essential fatty acids in macrophages, Prostaglandins Leukot Essent Fat. Acids 79 (2008) 123–129, https://doi.org/10.1016/j.plefa.2008.09.021.

[48] J.R. Montenegro-burke, J.A. Sutton, L.M. Rogers, L. Ginger, J.A. Mclean, D.M. Aronoff, Lipid profiling of polarized human monocyte-derived macrophages, Prostaglandins Other Lipid Mediat. (2016) 1–20.

[49] C. Zhang, Y. Wang, F. Wa, Z. Wang, Y. Lu, Y. Xu, K. Wang, Quantitative profiling of glycerophospholipids during mouse and human macrophage differentiation using targeted mass spectrometry, Sci. Rep. 7 (2017) 1–13, https://doi.org/10.1038/s41598-017-00341-2.

[50] S. Wallner, M. Grandl, T. Konovalova, A. Sigru, T. Kopf, M. Peer, E. Orso, G. Liebisch, G. Schmitz, Monocyte to macrophage differentiation goes along with modulation of the plasmalogen pattern through transcriptional regulation, PLoS One 9 (2014), https://doi.org/10.1371/journal.pone.0094102 e94102.

[51] A. Scaccabarozzi, P. Arosio, G. Weiss, L. Valenti, P. Dongiovanni, A.L. Fracanzani, M. Mattioli, S. Levi, G. Fiorelli, S. Fargion, Relationship between TNF-a and iron metabolism in differentiating human monocytic THP-1 cells, Blood 110 (2000) 978–984, https://doi.org/10.1046/j.1365-2141.2000.02280.x.

[52] S.T. Kinik, A.M. Tuncer, Ç. Altay, Transferrin receptor on peripheral blood lymphocytes in iron deficiency anaemia, Br. J. Haematol. 104 (1999) 494–498, https://doi.org/10.1046/j.1365-2141.1999.01226.x.

[53] F. Gatto, R. Cagliani, T. Catelani, D. Guarnieri, M. Moglianetti, P.P. Pompa, G. Bardi, PMA-induced THP-1 macrophage differentiation is not impaired by citrate-coated platinum nanoparticles, Nanomaterials 7 (2017) 1–10, https://doi.org/10.3390/nano7100332.

[54] E.K. Park, H.S. Jung, H.I. Yang, M.C. Yoo, C. Kim, K.S. Kim, Optimized THP-1 differentiation is required for the detection of responses to weak stimuli, Inflamm. Res. 56 (2007) 45–50, https://doi.org/10.1007/s00011-007-6115-5.

[55] N. Molaae, G. Mosayebi, A. Pishdadian, M. Ejtehadifar, A. Ganji, Evaluating the proliferation of human peripheralblood mononuclear cells using MTT assay, Int. J. Basic Sci. Med. 2 (2017) 25–28. https://doi.org/10.15171/ijbsm.2017.06.

[56] K.E. Sullivan, J. Cutilli, L.M. Piliero, D. Ghavimi-Alagha, S.E. Starr, D.E. Campbell, S.D. Douglas, Measurement of cytokine secretion, intracellular protein expression, and mRNA in resting and stimulated peripheral blood mononuclear cells, Clin. Diagn. Lab. Immunol. 7 (2000) 920–924, https://doi.org/10.1128/CDLI.7.6.920-924.2000.